Fine Chemical Engineering
http://ojs.wiserpub.com/index.php/FCE/

Research Article

Di-hydrogen Storage in Novel $(C_nGe_n)_2$ Nanostructures: Theoretical Study at Density Functional Theory (DFT) Level

Sellam Djamila[1], Elkebich Moumena[2], Arbia Yassamina[2], Brahimi Meziane[2*]

[1]Laboratory of Applied Chemistry and Engineering, Mouloud Mammeri University, Tizi Ouzou, Algeria
[2]Laboratory of Theoretical Physical Chemistry and Informatics Chemistry, University of Sciences and Technology Houari Boumediene, Algiers, Algeria
E-mail: m.brahimi@usthb.dz

Received: 21 August 2024; **Revised:** 23 November 2024; **Accepted:** 5 December 2024

Abstract: The Di-hydrogen solid-state is formed only at very low temperatures and pressures exceeding 1.5 million atmospheres. These draconian conditions are harmful to the economic and safe use of hydrogen, even if several studies refer to solid hydrogen which in reality is hydrogen adsorbed or absorbed on metallic surfaces or other. The objective of this research is to find new nanostructures with cages form that are able to confine a larger number of hydrogen molecules, potentially suggesting the geometry of the unit cell of solid hydrogen under standard conditions of (P, T). For this purpose, we use the density functional theory (DFT) method with the B3LYP and ωB97XD functional with the 6-31+G* basis. The MP2/6-311G++(d,p) level leads to the same results. The calculations of energies formation, infrared (IR) spectra, the shape of the molecular orbitals frontiers (MOF) and the Energy Gap will be done at theoretical level. These cage nanostructures are potential candidates for the Di-hydrogen storage. The $2H_2$ complex adopts a planar geometry, whereas $3H_2$ assumes a bi-pyramidal geometry with a square base.

***Keywords*:** new cage structure $(C_nGe_n)_2$, DFT, Di-hydrogen solid-state, hydrogen-molecule storage

1. Introduction

Fossil energy has received growing interest during the last ten decades due to its advantageous characteristics. However, fossil fuels are very polluting and non-renewable.[1] The oil crisis of 1973 has considerably directed the search for new alternatives. Thus, Di-hydrogen has become a strategic energy option; it is, today, a credible alternative to fossil fuels such as oil or gas. For the same quantity, Di-hydrogen has a higher thermodynamic density than conventional fossil fuels (one kilogram of hydrogen provides the same energy as about 3 kg of oil).[2] However, the energy cost of hydrogen production is estimated to be 2.9 times that of hydrocarbons, without taking into account the polluting effect of the latter.[3] Hydrogen also faces several challenges for large-scale use: (i) high energy consumption in its extraction and processing, (ii) difficulty in storage, (iii) flammable instability and flammability. These three major constraints make this fuel dangerous and difficult to exploit. The ultimate goal is to produce green non-polluting Di-hydrogen using solar energy.[1,2] In the meantime, the best solution would be solid Di-hydrogen,[4] which is produced under extreme conditions at approximately 120 K and 1.5 million atmospheres.

It becomes the only alternative to its exploitation and uses at a large scale.[5] Solid-state hydrogen storage is possible

DOI: https://doi.org/10.37256/fce.6120255548

through two different processes, adsorption,[6-9] and absorption.[10-12] In both cases, calling this "Solid hydrogen" is somewhat misleading, in reality, the hydrogen remains in gaseous state, adsorbed or absorbed by a solid material.

In this work, we propose an alternative approach to the Di-hydrogen storage using novel nanostructures in the form of cages composed of carbon and germanium atoms. The study was done using density functional theory (DFT) level with the B3LYP,[13-16] and ωB97XD functional that uses a version of Grimme's D2 dispersion model and the 6-31+G* basis.[17]

2. Theoretical methodology

The density functional theory (DFT) calculations have been executed using the Gaussian 09 package.[18] Geometry optimizations and property calculations on $(C_nGe_n)_2$ (n = 6, 7, and 8) and $(C_nGe_n)_2@mH_2$ (m = 2, and 3) structures were carried out with the B3LYP non-local hybrid functional,[13] which is reported to be quite reliable in describing the potential energy surface (PES) of similar structures.[19] Furthermore, ad hoc calculations on similar structures were carried out by Elkebich et al. which show that the Moller-Plesset MP2/6-31+G(d,p) level leads to the same results as the DFT level with the B3LYP functional.[20] Symmetry constraint was not imposed during the geometry optimization. All stationary points were confirmed through calculations on the involved cage structure using DFT level with hybrid functional B3LYP, PBE1PBE,[21-22] ωB97XD,[17] and 6-31+G* basis sets. All normal modes are confirmed to be real using tight key word for the convergence criterion.

The highest occupied molecular orbital (HOMO) and lowest unoccupied molecular orbital (LUMO) are the principal orbital taking part in chemical stability and chemical reactions. HOMO and LUMO energies are directly related to the electron affinity (EA) and the ionization potential (IP).[23] The difference between LUMO and HOMO energies is a gap energy $\Delta E = |E_{LUMO} - E_{HOMO}|$. Atomic polarizability tensor (APT) is interpreted as sum of the charge tensor and charge flux tensor, leading to charge-charge flux model.[24]

Additionally, the formation energy E_F of $(C_6Ge_6)_2$ cage structures was also calculated as defined in the following equation:[25]

$$E_F = E_T - n_{Ge} \cdot E_{Ge} - n_c \cdot E_C \quad (1)$$

where, E_T is the total energy of cages molecules, n_{Ge}, and n_C are the numbers of Ge, and C atoms, respectively. E_{Ge}, and E_C are the energies, determined at the same level of theory, of an isolated Ge, and C atom, respectively. In all cases, we considered the zero-point energy correction (ZPEC).[26]

3. Results and discussion

3.1 *Structural, energetic, and infra red properties*

Many authors have synthesized and studied theoretically new molecular structures and nanostructure able to adsorb or absorb one or more hydrogen molecules.[27-31] In this context, we propose new cage-structure molecules composed of carbon and germanium atoms (see Figure 1). Calculation of the formation energies, using the relation (1) leads to strongly negative values for the species $(C_nGe_n)_2$ (n = 6, 7 and 8). The values are equal, respectively, for $(C_6Ge_6)_2$ to -14,280 kJ/mol, at the level B3LYP/6-31+G*, we find the same order of magnitude with the functional ωB97XD/6-31+G* which takes into account the dispersion energies as defined by Grimme.[17] The $(C_6Ge_6)_2$ species is formed by 42 bonds (12 CC, 12 CGe, and 18 GeGe bonds), if these latter are identical, the average energy per bond would be around -340.16 kJ/mol. This value is between that of H_2 (-435.14 kJ/mol), and Cl_2 (-243.09 kJ/mol) or C-S (-269.62 kJ/mol). For that, this new structure would be stable, and could be synthesized experimentally.

The optimization of the geometries, without constraints on symmetries, leads to normal modes of vibration which are all real. The stable molecular geometries are given in Figure 1. The structure of $(C_8Ge_8)_2$ is slightly flattened.

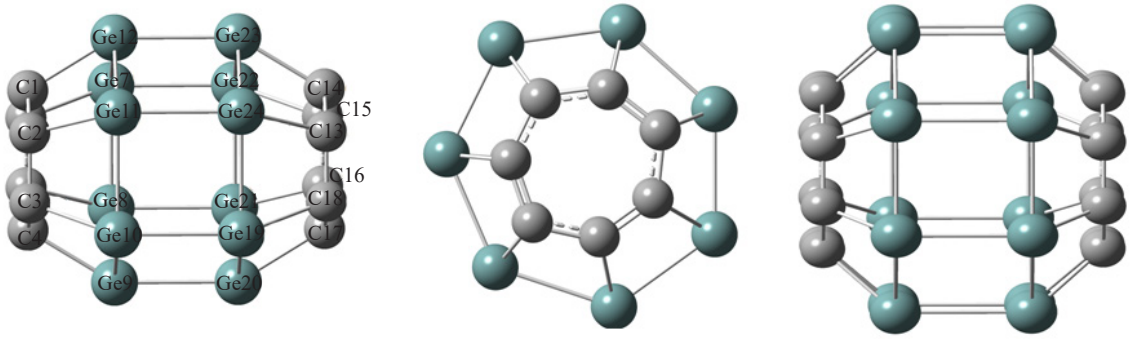

(a): $(C_6Ge_6)_2$ $E_{elec + ZPEC}$ = -25,261.186535 | (b): $(C_7Ge_7)_2$ -29,471.336059 | (c): $(C_8Ge_8)_2$ -33,681.525418 u.a

Figure 1. Optimized geometry of $(C_nGe_n)_2$ (n = 6, 7, and 8) species with sum of electronic energies and zero point energy correction (ZPEC)[26]

Both cage structures have zero dipole moments, with all C and Ge atoms hybridized in sp^3, and the respective carbon and germanium atoms are in the same plane as if they were hybridized in sp^2. This aspect, of hybridization of the C and Ge atom, is discussed by Elkebich et al.[20]

These new structures, with form of cage, can confine Di-hydrogen at room temperature and atmospheric pressure. Complete geometry optimization (without symmetry constraints) of the $(C_nGe_n)_2@mH_2$ species with (n = 6, 7, 8, and m = 2, 3), leads to optimal geometries with all the normal modes of vibration being real. The geometry of the $(C_6Ge_6)_2@mH_2$ species (m = 2 and 3) are shown in Figure 2. Energy dispersion decreases as the number of confined hydrogen molecules. The difference between $(C_6Ge_6)_2@2H_2$ (-183.13 kJ/mol) and $(C_6Ge_6)_2$ (-146.52 kJ/mol) is equal to -36.61 kJ/mol. The same tendency is observed for the three confined molecules in the $(C_6Ge_6)_2@3H_2$ species. The species $(C_nGe_n)_2@mH_2$ (n = 7, 8, and m = 2, and 3) lead to the same results.

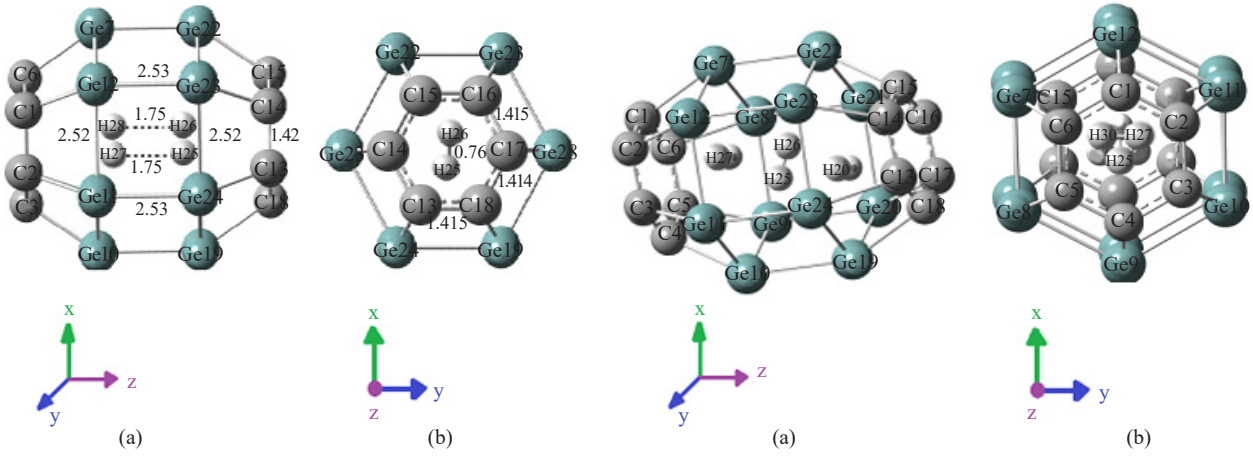

(a) (b) (a) (b)

$(C_6Ge_6)_2@2H_2$ $(C_6Ge_6)_2@3H_2$

Figure 2. Optimized species $(C_6Ge_6)_2@mH_2$ (m = 2 and 3) with (a) = side view; (b): top view

While the H_2 molecule is not active in infrared (IR) spectroscopy, it becomes IR-active in the $(C_6Ge_6)_2@2H_2$ complex, as it is in germanium and carbon nanotubes.[32-33] The IR spectrum of the $(C_6Ge_6)_2@mH_2$ complex, with m = 0, 2, and 3, is depicted in Figure 3. The most intense frequencies correspond to the symmetrical displacement, in the same direction, of the four hydrogen atoms.

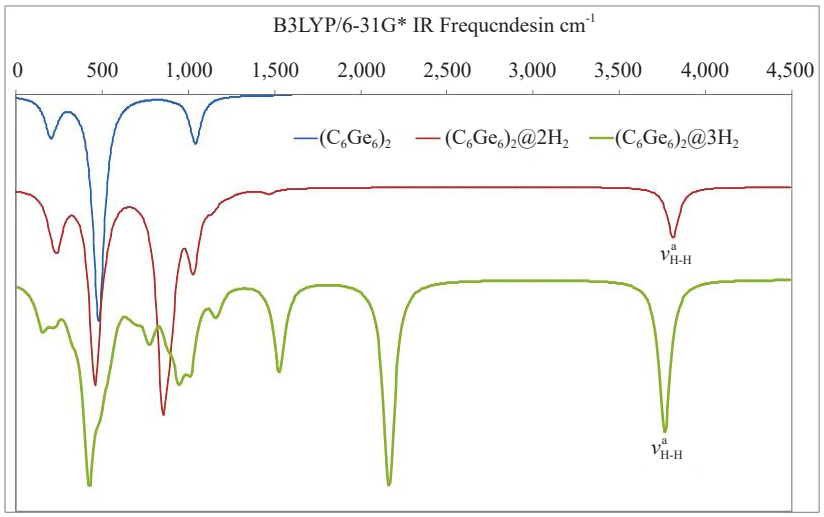

Figure 3. IR spectra of $(C_6Ge_6)_2@mH_2$ (m = 0 (blue), 2 (red), 3(green)), obtained at the B3LYP/6-31+G* level. For more clarity, the area under the peaks is multiplied by 10

The frequencies, corresponding to the symmetric IR displacement vectors given in Figure 4(a), at 498 for $(C_6Ge_6)_2@0H_2$, 487 for $(C_6Ge_6)_2@2H_2$, and 453 cm^{-1} for $(C_6Ge_6)_2@3H_2$ appear for all species. These frequencies decrease when the number of hydrogen molecule increases. For the anti-symmetric IR displacement, given in Figure 4(b), we obtain 488 cm^{-1} for $(C_6Ge_6)_2@0H_2$, 459 cm^{-1} for $(C_6Ge_6)_2@2H_2$, and 423 cm^{-1} for $(C_6Ge_6)_2@3H_2$. The same conclusions are obtained when the cage length increases.

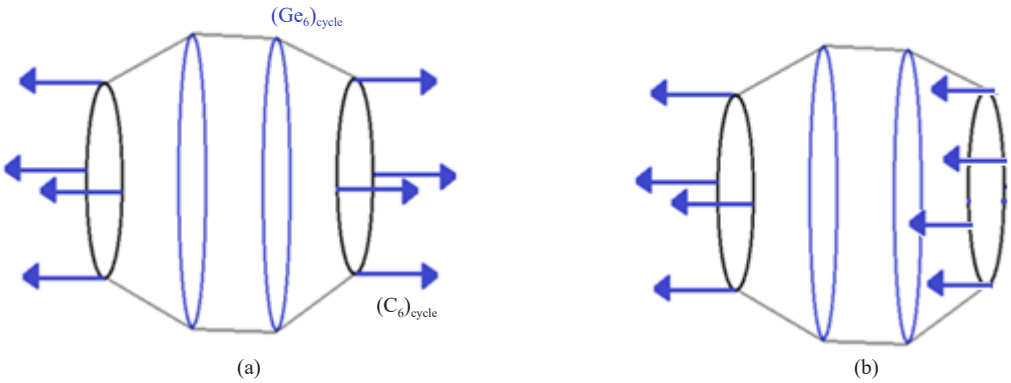

Figure 4. IR displacement vectors, (a) symmetric, and (b) anti-symmetric displacement

The number of frequencies involving the hydrogen molecules increases with the number of these molecules. A vibrational mode characteristic of the presence of $2H_2$ (intense anti-symmetric elongation of the two bonds H-H, $\nu^a_{H\text{-}H}$) appears at 3,810 cm^{-1} (see Figure 5(b)). The area under the curve of IR spectra shown in Figure 3 is proportional to the number of H_2 molecules in the cage.

For the species $(C_6Ge_6)_2@3H_2$, two additional normal modes of vibration correspond to the symmetrical elongation of the two extreme hydrogen molecules and a strong anti-symmetrical at 2,163 cm^{-1} and 1,528 cm^{-1}, respectively (see the IR displacement vectors shown in Figure 5(a)). Anti-symmetric elongation of the two external bonds H-H, $\nu^a_{H\text{-}H}$, appears at 3,762 cm^{-1} with a shift towards low frequencies of 38 cm^{-1}.

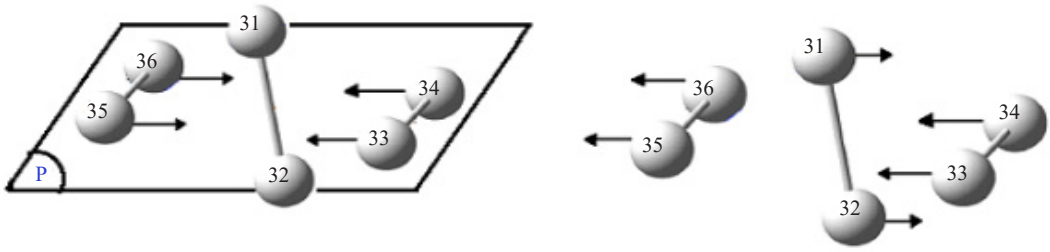

1,528 cm^{-1} 2,163 cm^{-1}

(a)

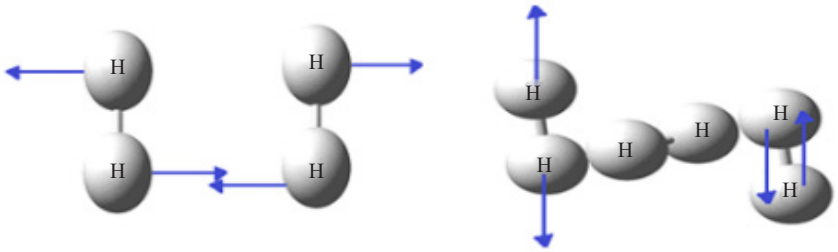

3,810 cm^{-1} 3,762 cm^{-1}

(b)

Figure 5. (a): IR displacement vectors for 1,528 cm^{-1}, and 2,163 cm^{-1}. These atom numbers (33, 34, 35, and 36) are in the same plane (P). (b): Hydrogen IR displacement vectors for 3,810 cm^{-1} in $(C_6Ge_6)_2@2H_2$, and for 3,762 cm^{-1} in $(C_6Ge_6)_2@3H_2$

The confined hydrogen becomes active in IR because of the APT charges that appear in the $(C_6Ge_6)_2@mH_2$ complex (see Figure 6) and because of the interlocking Van der Waals radii of the different atoms of the complex (see Figure 7).[23] The interactions between the germanium atoms of the cages and the confined hydrogen molecules lead to a change in polarity of the latter (see APT charge) enhancing their IR visibility and contribution to their stability.

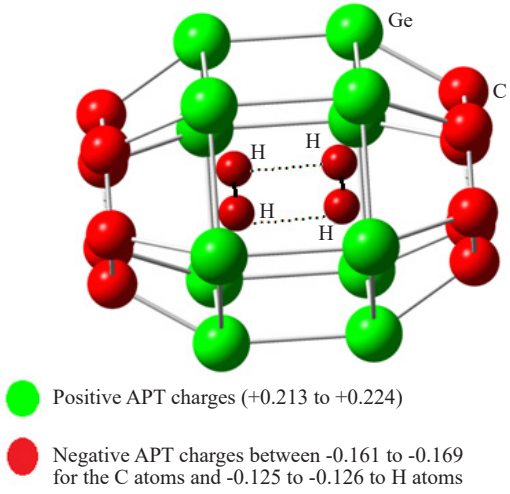

Figure 6. APT charges of $(C_6Ge_6)_2@2H_2$

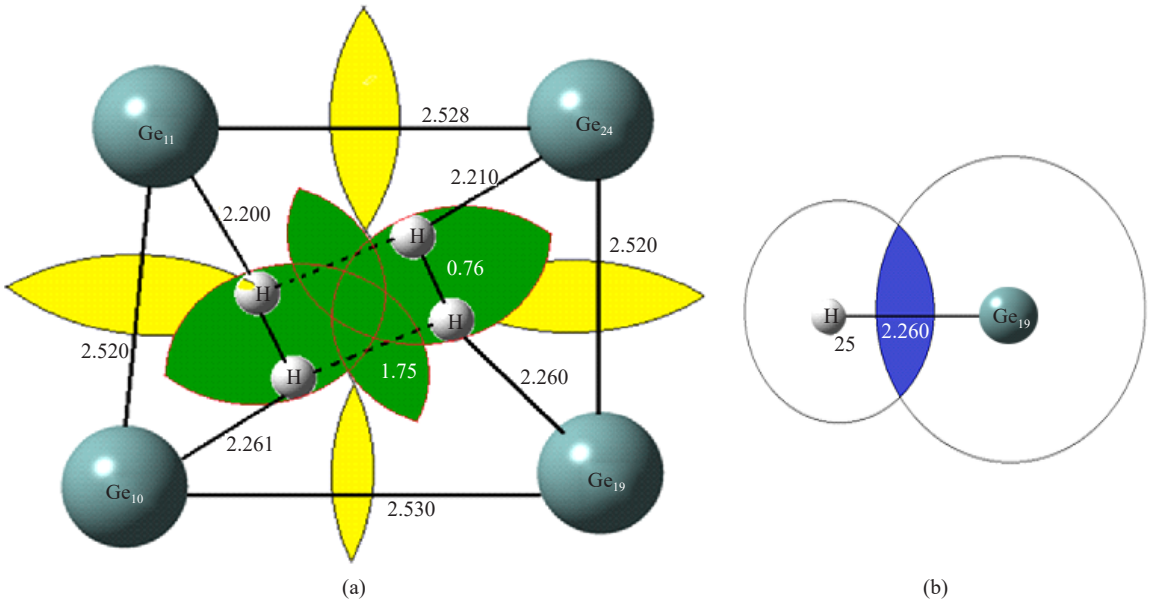

Figure 7. Van der Waals overlap, (a) in yellow between the germanium atoms, and green between the hydrogen atoms; (b) between the germanium atom 19, and the hydrogen atom 25. The Van der Waals radii of different atoms are: R^{H}_{VdW} = 1.20 Å; R^{C}_{VdW} = 1.70 Å; R^{Ge}_{VdW} = 2.11 Å

The $2H_2$ complex confined in $(C_6Ge_6)_2$ is located in the middle of the cage. It is centred compared to the benzene and with an angle of 25 degrees between the two planes carrying respectively the germanium atoms (8, 11, 24, and 21) and the hydrogen atoms (25, 26, 27, and 28) (see Figure 8). When this configuration is optimized in the isolated state, at the same level of theory, it does not correspond to an energy minimum. The two hydrogen molecules move away from each other.

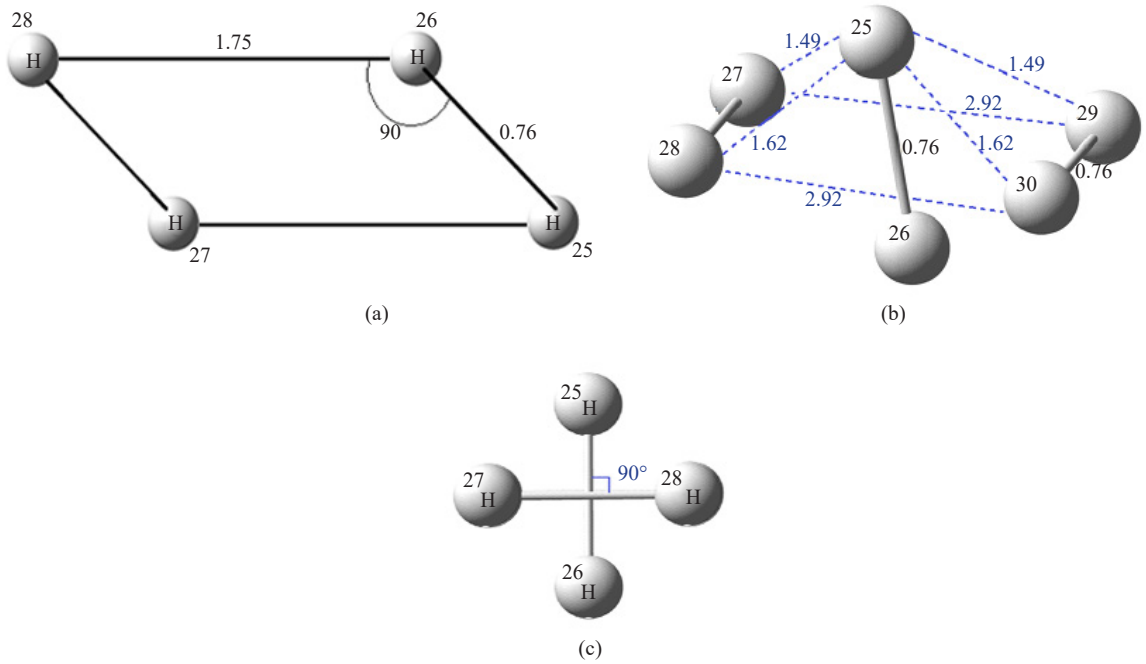

Figure 8. (a) $2H_2$ geometry complex in $(C_6Ge_6)_2@2H_2$, and (b) $3H_2$ in $(C_6Ge_6)_2@3H_2$ side views where the atom numbers (27, 28, 29, and 30) are in the same plane, and (c) Top view where the atom numbers (25 and 26) are in the plane which is perpendicular to the first one

When a third hydrogen molecule is introduced into $(C_6Ge_6)_2$, these are placed as shown in Figure 2. The $3H_2$ complex, formed inside the cage, is given in Figure 8 (b) and (c). The molecule H_{25}-H_{26} with a distance of 0.76 Å is located in a plane that is perpendicular to the one that carries the two molecules H_{27}-H_{28}, and H_{29}-H_{30}. The whole forms a bi-pyramidal geometry with an asymmetric square base, the distances (25, 27), and (25, 29) (1.49 Å) are different from (25, 29) and (25, 30) (1.62 Å). The H-H interatomic distance, in all the complexes which confine mH_2, is of the order of 0.76 Å. It is similar to that obtained by Bai et al. Inside the Lithium-Decorated Borospherene B_{40} nanostructures.[34]

When we optimize the $3H_2$ complex in the isolated state, it dislocates, showing that its stability is due to the confinement in the new proposed cage structures. We observe the same conclusions when the size of the cages increases. On the other hand, the number of confined Di-hydrogen molecules increases with the size of the cages. Lengthening the cage by adding 6 Ge atoms that encapsulates $3H_2$, conduces to the optimal geometry presented in Figure 9.

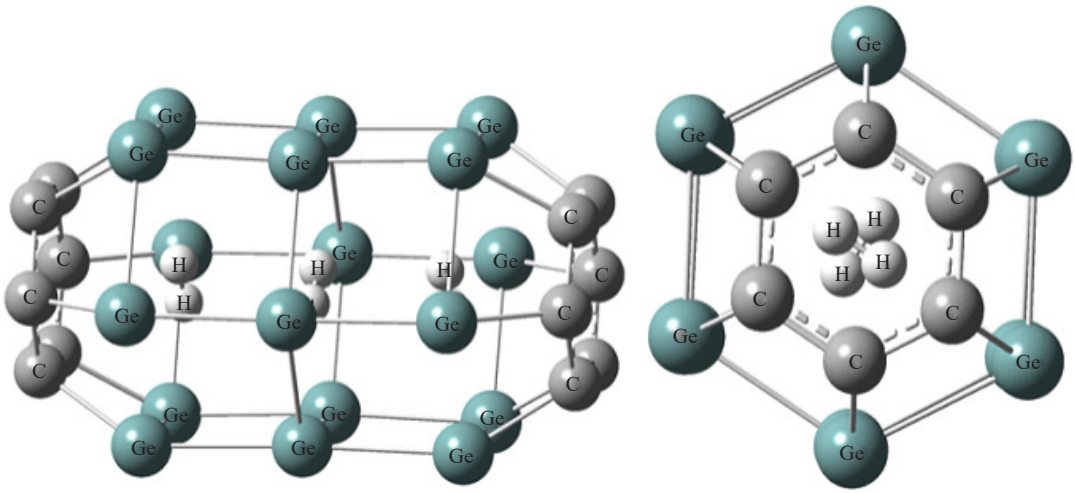

$(C_6\text{-}(Ge_6)_2\text{-}Ge_6)@3H_2$

Figure 9. Optimized species $(C_6\text{-}(Ge_6)_2\text{-}Ge_6)@3H_2$ with (a) side view; (b) top view

In the complex $(C_6\text{-}(Ge_6)_2\text{-}Ge_6)@3H_2$, the six hydrogen atoms occupy the summits of a bi-pyramid with a symmetrical square base (see Figure 10).

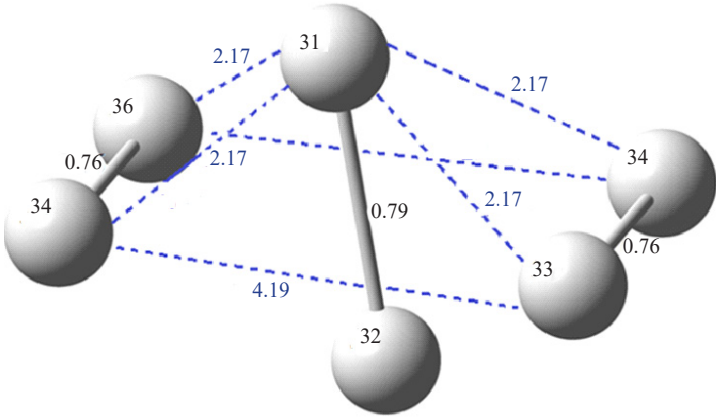

Figure 10. $3H_2$ in $(C_6\text{-}(Ge_6)_2\text{-}Ge_6)@3H_2$. The atom numbers (33, 34, 35, and 36) are in the same plane, and number (31 and 32) are in the plane which is perpendicular to the first one. The distances are in Å

The confinement of three hydrogen molecules, in the complex $(C_6\text{-}(Ge_6)_2\text{-}Ge_6)@3H_2$, shortens the C-C bonds by 0.01 Å and Ge-Ge by 0.11 Å, lengthens the C-Ge bonds by 0.01 Å, decreases the length of the cage by 0.13 Å and decreases the diameter of the cage by 0.08 Å (see Figure 11). Thus, the stabilizing interactions of the hydrogen molecules in the cage are in agreement with the dispersion energy, which decreases when the number of confined hydrogen molecules increases.

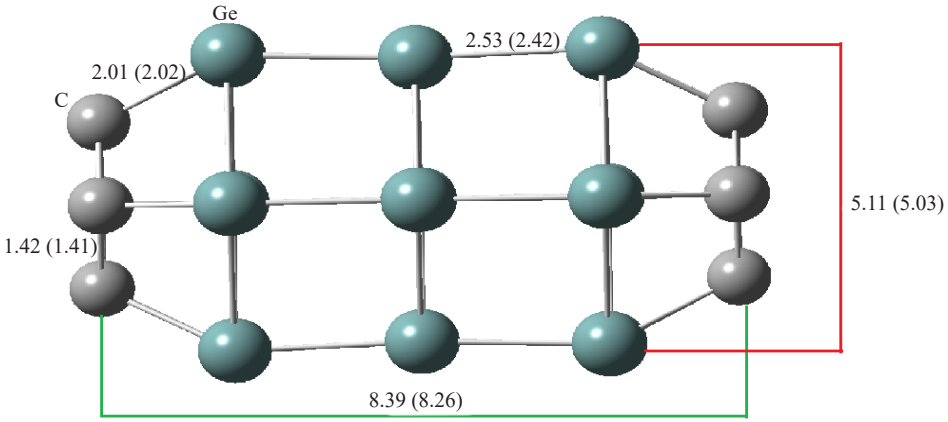

Figure 11. Distances in Å without hydrogen molecules, and in parenthesis with tree hydrogen molecules obtained at the ωB97XD/6-31+G* level

The calculation at the Post-Hartree-Fock level (MP2/6-311++G**) for the $(C_6Ge_6)_2$ and $(C_6Ge_6)_2@3H_2$ complexes leads to the same results as the ωB97XD/6-31+G* level, the errors are of the order of ± 0.01Å for the bond length, and of the order of ± 2 degrees for the angles.

3.2 *Molecular orbital frontiers (MOF)*

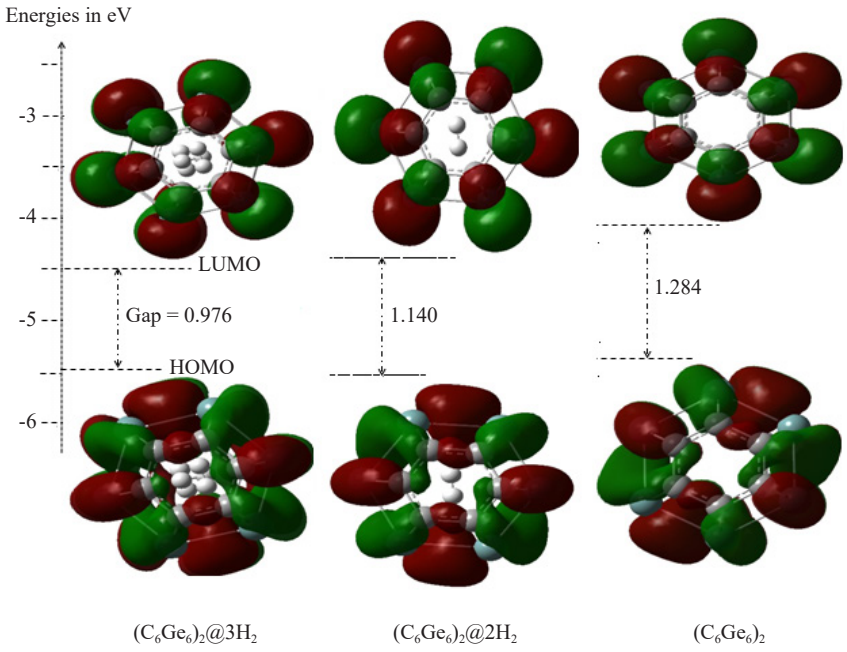

Figure 12. MOF and gap energies of $(C_6Ge_6)_2$

The molecular orbitals frontiers (MOF) plotted in Figure 12, show that for all cages, with an even number of C and Ge atoms, the HOMO is primarily localized on the bonds while the LUMO is localized on the atoms. For the $(C_7Ge_7)_2$ structure, with an odd number of C and Ge atoms, the trend is reversed.

The different forms of the MOFs of $(C_6Ge_6)_2@mH_2$ species (m = 0, 2, 3) are plotted in Figure 11. The MOFs, with confined mH_2 molecules, remain the same as for the empty cages. The only change is the volume of the MOFs which become more noticeable and do not involve the confined hydrogen molecules. We obtain the same tendency for the species $(C_7Ge_7)_2@mH_2$ and $(C_8Ge_8)_2@mH_2$. The energy gap, for the $(C_6Ge_6)_2@3H_2$ complex is 0.976 eV (see Figure 12), it decreases to 0.826 eV when the cage $(C_6\text{-}(Ge_6)_2\text{-}Ge_6)@3H_2$ (see Figure 9) is lengthened. This reduction in energy gap suggests that the complex becomes more reactive, which would likely result in the rapid release of hydrogen molecules. Furthermore, the energy gap increases as the cage diameter increases, with values of 0.976 eV for $(C_6Ge_6)_2@3H_2$ and 1.323 eV for $(C_8Ge_8)_2@3H_2$.

4. Conclusion

The present theoretical study, conducted at the level of density functional theory with the B3LYP and ωB97XP functional using the 6-31+G* basis, allows us to argue that the species $(C_nGe_n)_2$ with n = 6, 7, and 8 are, both stable and likely to exist or be synthesized. Furthermore, these species are potential candidates for the storage of Di-hydrogen under standard conditions of pressure and temperature. The mH_2 complexes (with m = 2, 3) confined inside $(C_nGe_n)_2$ are stable and can be highlighted by IR spectroscopy with different characteristic frequencies. The $2H_2$ complex adopts a planar geometry whereas $3H_2$ adopts a bi-pyramidal geometry with a square base. This bipyramidal arrangement (bi-pyramid with square base) of the three hydrogen molecules is, in our opinion, the unit cell of solid hydrogen at standard pressure and temperature. The IR spectrum also provides insight into the number of hydrogen molecules confined in the new structure.

Author contributions

All authors contributed to the study's conception. Djamila Sellam performed the literature survey and the writing of the manuscript. Moumena Elkebich and Yassamina Arbia performed the DFT calculations. Meziane Brahimi performed the literature and calculations survey, and the writing of the manuscript.

Conflict of interest

The authors declare that they have no competing financial interests.

References

[1] Veziroglu, T. N. *Int. J. Hydrogen Energy*. **1987,** *12*, 99.
[2] Momirlan, M.; Veziroglu, T. N. *Renew. Sustain. Energy Rev*. **2002,** *6*, 141-179.
[3] Edwards, P. P.; Hensel, F. *Nature* **1997,** *388*, 621-621.
[4] Yurum, Y. Hydrogen energy system: Production and utilization of hydrogen and future aspects. In *NATO ASI Series, Serie E: Applied Sciences-v. 295*; Springer Science & Business Media, 1995.
[5] Salman, M. S.; Rambhujun, N.; Pratthana, C.; Lai, Q.; Sapkota, P.; Aguey-Zinsou, K.-F. Chapter 12: Solid-state hydrogen storage as a future renewable energy technology. In *Micro and Nano Technologies, Nano Tools and Devices for Enhanced Renewable Energy*; Devasahayam, S.; Mustansar, H-C., Eds.; Elsevier, 2021; pp 263-287.
[6] Jain, V.; Kandasubramanian, B. *J. Mater. Sci*. **2020,** *55*, 1865-1903.
[7] Bannenberg, L. J.; Heere, M.; Benzidi, H.; Montero, J.; Dematteis, E. M.; Suwarno, S.; Jaroń, T.; Winny, M.; Orłowski, P. A.; Wegner, W.; Starobrat, A.; Fijałkowski, K. J.; Grochala, W.; Qian, Z.; Bonnet, J.-P.; Nuta, I.;

Lohstroh, W.; Zlotea, C.; Mounkachi, O.; Cuevas, F.; Chatillon, C.; Latroche, M.; Fichtner, M.; Baricco, M.; Hauback, B. C.; El Kharbachi, A. *Int. J. Hydrogen Energy*. **2020,** *45*(58): 33687-33730.
[8] Broom, D. P.; Webb, C. J.; Hurst, K. E.; Parilla, P. A.; Gennett, T.; Brown, C. M.; Zacharia, R.; Tylianakis, E.; Klontzas, E.; Froudakis, G. E.; Steriotis, Th. A.; Trikalitis, P. N.; Anton, D. L.; Hardy, B.; Tamburello, D.; Corgnale, C.; van Hassel, B. A.; Cossement, D.; Chahine, R.; Hirscher, M. *Appl. Phys. A* **2016,** *122*, 151.
[9] Chen, Y.-S.; Gua, J.-J.; Liu, P.-B.; Zhao, H-.Y.; Wang, J.; Liu, Y. *Physica Scripta* **2023,** *4*, 045409.
[10] Hu, J.; Zhang, J.; Xiao, H.; Xie, L.; Shen, H.; Li, P.; Zhang, J.; Gong, H.; Zu, X. *Inorg. Chem*. **2020,** *59*(14), 9774-9782.
[11] Ding, Z.; Li, H.; Shaw, L. *Chemical Eng. J*. **2020,** *385*, 123856.
[12] Lewis, S. D.; Chippar, P. *Energy* **2020,** *194*, 116942.
[13] Becke, A. D. *Phys. Rev. A*. **1988,** *38*(6), 3098.
[14] Kim, K.; Jordan, K. D. *J. Phys. Chem*. **1994,** *98*(40), 10089-10094.
[15] Stephens, P. J.; Devlin, F. J.; Chabalowski, C. F.; Frisch, M. J. *J. Phys. Chem*. **1994,** *98*(45), 11623-11627.
[16] Cramer, C. J. *Essentials of Computational Chemistry: Theories and Models, 2nd Edition*; Wiley, 2004.
[17] Yanai, T.; Tew, D. P.; Handy, N. C. *Chem. Phys. Lett.* **2004,** *393*, 51-57.
[18] Frisch, M. J.; Trucks, G. W.; Schlegel, H. B.; Scuseria, G. E.; Robb, M. A.; Cheeseman, J. R.; Scalmani, G.; Barone, V.; Mennucci, B.; Petersson, G. A. *Gaussian 09, Revision A.02*; Gaussian, Inc.: Wallingford CT, 2016.
[19] Chattaraj, P. K.; Sarkar, U.; Roy, D. R. *Chem. Rev*. **2006,** *106*, 2065.
[20] Elkebich, M.; Zaater, S.; Abtouche, S.; Brahimi, M. *Bull. Mater. Sci*. **2020,** *43*, 160.
[21] Perdew, J. P.; Burke, K.; Ernzerhof, M. *Phys. Rev. Lett*. **1996,** *77*, 3865.
[22] Perdew, J. P.; Burke, K.; Ernzerhof, M. *Phys. Rev. Lett*. **1997,** *78*, 1396.
[23] Zeyrek, C. T.; Unver, H.; Arpaci, Ö. T.; Polat, K.; İskeleli, N. O.; Yildiz, M. *J. Mol. Struct*. **2015,** *1081*, 22-37.
[24] Yadav, R. A.; Singh, S.; Srivstava, M. *Pharma. Analyt. Acta*. **2015,** *6*, 2-16.
[25] Kassaee, M. Z.; Rad, H. A. *Comput. Mater. Sci*. **2010,** *48*, 144-149.
[26] Wong, K. Y.; Gao, J. *J. Chem. Theory. Comput*. **2008,** *4*(9), 1409-1422.
[27] Ucida, K.; Kishimoto, N.; Noro, S. I.; Iguch, H.; Takaishi, S. *Dalton Trans*. **2021,** *50*, 12630-12634.
[28] Chakraborty, R.; Carsch, K. M.; Jaramillo, D. E.; Yabuuchi, Y.; Furukawa, H.; Long, J. R.; Head-Gordon, M. *J. Phys. Chem. Lett*. **2022,** *13*(44), 10471-10478.
[29] Wang, K.; Chen, W.; Li, L. *Renew. Energy* **2022,** *187*, 1118-1129.
[30] Sarmah, K.; Rohman, S. S.; Purkayastha, S. K.; Kalita, A. J.; Guha, A. K. *Phys. Chem. Chem. Phys*. **2022,** *46*, 28577-28583.
[31] Siviero, G.; Bello, V.; Mattei, G.; Mazzoli, P.; Battaglin, G.; Checchetto, R.; Miotello, A. *Int. J. Hydrogen Energy* **2009,** *34*, 4817-4826.
[32] Djitli, W.; Abdelatif, M. L.; Belmiloud, Y.; Abdeldjebar, H.; Brahimi M.; Tangour, B. *Superlattices Microstruct*. **2018,** *122*, 596-607.
[33] Gtari, W. F.; Tangour, B. A. *Int. J. Quant. Chem*. **2013,** *113*, 2397-2404.
[34] Bai, H.; Bai, B.; Zhang, L.; Huang, W.; Mu, Y.-W.; Zhai, H.-J.; Li, S.-D. *Sci. Rep*. **2016,** *6*, 35518.